01 May 2004

Pulse Train Control Technique for Flyback Converter

Mark Telefus

Anatoly Shteynberg

Mehdi Ferdowsi
Missouri University of Science and Technology, ferdowsi@mst.edu

Ali Emadi

Recommended Citation

M. Telefus et al., "Pulse Train Control Technique for Flyback Converter," *IEEE Transactions on Power Electronics*, vol. 19, no. 3, pp. 757-764, Institute of Electrical and Electronics Engineers (IEEE), May 2004. The definitive version is available at https://doi.org/10.1109/TPEL.2004.826498

Pulse Train Control Technique for Flyback Converter

Mark Telefus, Anatoly Shteynberg, *Member, IEEE*, Mehdi Ferdowsi, *Student Member, IEEE*, and Ali Emadi, *Senior Member, IEEE*

***Abstract*—Pulse Train™ control technique is introduced and applied to Flyback converter operating in discontinuous conduction mode (DCM). In contrast to the conventional pulse width modulation (PWM) control scheme, the principal idea of Pulse Train is to achieve output voltage regulation using high and low power pulses. The proposed technique is applicable to any converter operating in DCM. However, this work mainly focuses on Flyback topology. In this paper, the main mathematical concept of the new control algorithm is introduced and simulations as well as experimental results are presented.**

***Index Terms*—Critical conduction mode, dc–dc power converters, discontinuous conduction mode, flyback converter, near-zero-voltage switching, switch mode power supplies.**

I. Introduction

DUE TO HIGH efficiency and high power density as well as reduced costs, switched mode power supplies (SMPS) are now becoming more popular compared to the linear power supplies [1]. Since the number of semiconductor and magnetic components of Flyback converter is less than the other SMPS and, furthermore, it provides input/output isolation; therefore, this topology perfectly suits off-line low-cost power supply applications.

Flyback converter has been employed operating in both continuous conduction mode (CCM) and discontinuous conduction mode (DCM) as well as critical conduction mode, i.e., at the boundary between CCM and DCM [2], [3]. Critical conduction mode enjoys benefits such as zero current turn-on of the switch and zero current turn-off of the freewheeling diode. These soft switching transitions reduce the switching losses as well as the electromagnetic interference (EMI) noise [4]. Critical conduction mode has less current stress compared to DCM. Furthermore, the transfer function of the Flyback converter operating in critical conduction mode is first-ordered; thus, the feedback compensation is simplified compared to CCM. However, despite the advantageous benefits of critical conduction mode, its major drawback is the variations of the switching frequency of the converter as the output load changes.

This paper introduces Pulse Train™ control technique, which regulates the output voltage based on presence and absence of power and sense pulses and makes the Flyback converter operate in partial DCM and partial critical conduction mode. Not only does this control scheme offer a faster dynamic response compared with pulse width modulation (PWM) method, but also improves the efficiency by lowering the switch turn-on loss at the end of each power pulse based on choosing the right turn-on time instant. The required information for this action is provided from the measured signals of the converter during the sense pulses. This method is experimentally developed in iW2201, which is an 8-pin integrated circuit (IC). Pulse Train is simple, cost effective, and robust against the variations of the parameters of the converter. A method that shows some similarity to Pulse Train technique was recently introduced in [5] with inferior characteristics. To achieve fixed frequency operation, [5] proposes skip cycle modulation (SCM), which is basically an on/off control mode to regulate the output voltage. SCM method is based on constant width constant frequency pulse signals.

In this paper, Section II introduces the basic concepts of the new control algorithm. Section III investigates the stability of the proposed control scheme. In Section IV, a comprehensive analysis of the output voltage ripple is presented. Section V discusses the application of the near-zero-voltage switching technique for the purpose of efficiency improvement. Experimental results of applying Pulse Train technique on a Flyback converter are presented in Section VI. Smart skip mode and soft start are discussed in Sections VII and VIII, respectively. Finally, Section IX draws conclusions and presents an overall evaluation of this new control technique.

II. Pulse Train Control Scheme

Pulse Train control algorithm regulates the output voltage based on the presence and absence of power pulses, rather than employing PWM [6], [7]. Fig. 1 depicts the block diagram of the Pulse Train regulation scheme. If the output voltage is higher than the desired level, low-power *sense pulses* are generated sequentially until the desired voltage level is reached. On the other hand, if the output voltage is lower than the desired level, instead of sense pulses, high-power *power pulses* are generated. The time duration of the power and sense pulses are the same; but, due to the longer on time of the switch during a power pulse, compared to a sense pulse, more power will be delivered to the load. The ratio between the on-time duration of the switch in a power pulse and the on-time duration of the switch in a sense pulse (k) is chosen by making a compromise between the output voltage ripple and the power regulation range from full power to low power.

Fig. 2 depicts current waveform of magnetizing inductance of the transformer $L_{\rm m}$ after Pulse Train is being applied. At the beginning of each switching cycle, based on the difference of the output voltage with the desired voltage level, it will be determined whether a power or a sense pulse needs to be generated. Operating in constant peak current mode control, in a power pulse, the switch remains on and the primary current is

Manuscript received July 24, 2003; revised October 7, 2003. This work was supported by iWatt Corporation, Las Gatos, CA. Recommended by Associate Editor B. Fahimi.

M. Telefus and A. Shteynberg are with the iWatt Corporation, Las Gatos, CA 95032 USA.

M. Ferdowsi and A. Emadi are with the Electrical and Computer Engineering Department, Illinois Institute of Technology, Chicago, IL 60616-3793 USA (e-mail: emadi@iit.edu).

Digital Object Identifier 10.1109/TPEL.2004.826498

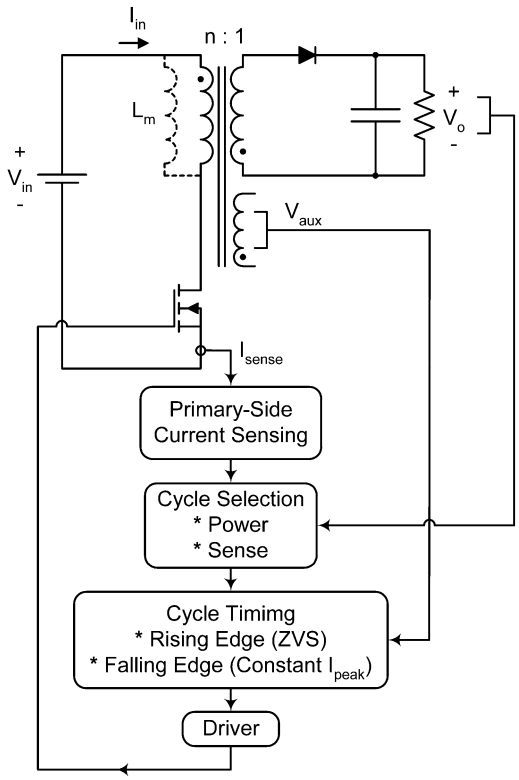

Fig. 1. Block diagram of pulse train control scheme.

allowed to increase until it reaches a designated constant peak level $(I_{\max})$. At this point, the switch turns off and the next cycle starts when the secondary current reaches zero. A sense pulse has the same period as the preceding power pulse; but the switch turns off when its current reaches $I_{\max}/k$. Since the primary current ramps linearly with the switch on time, the switch on-time duration of a sense pulse is $1/k$ times as the switch on-time duration of a power pulse. Hence, a sense pulse transfers just $1/k^2$ time as much energy as a power pulse. The controller measures the time duration of the power pulses and makes the subsequent sense pulses to have the same time duration; hence the switching frequency of the converter is fairly constant when the load changes.

Fig. 3 shows the simulation results of applying this control method on a Flyback converter with parameters defined in Table I. For this specific value of the output power demand, the control scheme generates two power pulses and one sense pulse in each regulation cycle.

Pulse Train enjoys on-line waveform analysis and hence, fast dynamic response. Fig. 4 compares the speed of response of Pulse Train with a typical PWM control to a step load change of 30% to 65% of full load. Arrows in this figure mark the time instant at which the step change has applied. As we can observe, Pulse Train has a much faster speed of response in contrast with PWM.

III. Stability Analysis

Considering a general switching period, as shown in Fig. 5, and based on the energy conservation rule, one can write

$$\Delta E_{\text{in}} = \Delta E_{L_{\text{m}}} + \Delta E_C + \Delta E_{\text{Load}} \tag{1}$$

where ΔE_{in} is the amount of energy that has been drawn from the input power source during the considered switching period. ΔE_{Lm} is the difference of the energy stored in the magnetizing inductance of the transformer and is equal to zero because L_{m} de-energizes at the end of each switching period. ΔE_C is the change of the energy stored in the output capacitor during the same switching period and can be described as

$$\Delta E_C = E_{C,(n+1)T} - E_{C,nT}. \tag{2}$$

And finally, ΔE_{Load} is the amount of energy delivered to load R during the same period. Output capacitor C provides the load current; hence, we can write

$$\Delta E_{\text{Load}} = \frac{1}{R} \cdot \int_{nT}^{(n+1)T} V_C^2 \cdot dt. \tag{3}$$

In (3), using the trapezoidal rule instead of integration, we can approximate ΔE_{Load} as

$$\Delta E_{\text{Load}} \cong \frac{T}{2R} \left(V_{C,(n+1)T}^2 + V_{C,nT}^2 \right). \tag{4}$$

Moreover, the energy stored in a capacitor at each instant is equal to the squared value of the voltage that appears across the capacitor divided by twice the value of the capacitor; hence, (4) can be rewritten as

$$\Delta E_{\text{Load}} \cong \frac{T}{RC} \left(E_{C,(n+1)T} + E_{C,nT} \right). \tag{5}$$

Substituting (2) and (5) into (1) and solving for the energy stored in the output capacitor at the end of the desired switching period, one obtains

$$E_{C,(n+1)T} = M \cdot E_{C,nT} + \frac{1}{1 + \frac{T}{RC}} \Delta E_{\text{in}} \tag{6}$$

where

$$M = \frac{1 - \frac{T}{RC}}{1 + \frac{T}{RC}} < 1. \tag{7}$$

Equation (6) shows the recursive relation of the energy stored in the output capacitor. We need to note that M is always less than one; therefore, the converter is stable under any pattern of power and sense pulses in the closed loop system. Using the input current, ΔE_{in} can be described as

$$\Delta E_{\text{in}} = E_{L_{\text{m}},nT+t_{\text{on}}} - E_{L_{\text{m}},nT} = L_{\text{m}} \cdot \int_0^{i_{in,nT+t_{\text{on}}}} i_{\text{in}} \cdot dt. \tag{8}$$

where as for a power pulse, we have

$$\Delta E_{\text{in}} = 0.5 L_{\text{m}} I_{\max}^2 \tag{9}$$

and for a sense pulse, we have

$$\Delta E_{\text{in}} = \frac{0.5 L_{\text{m}} I_{\max}^2}{k^2} \tag{10}$$

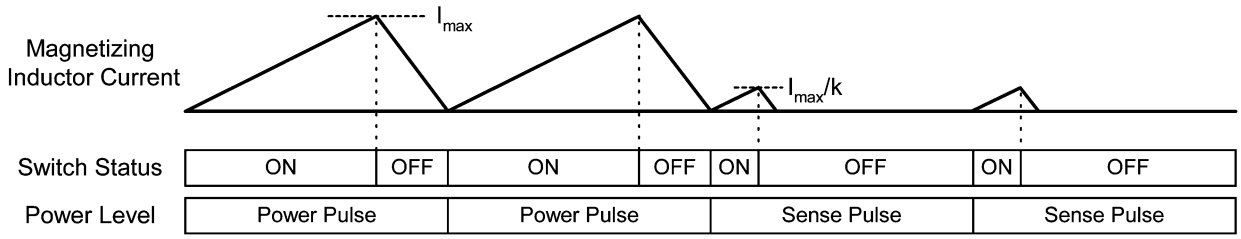

Fig. 2. Power and sense pulse cycles.

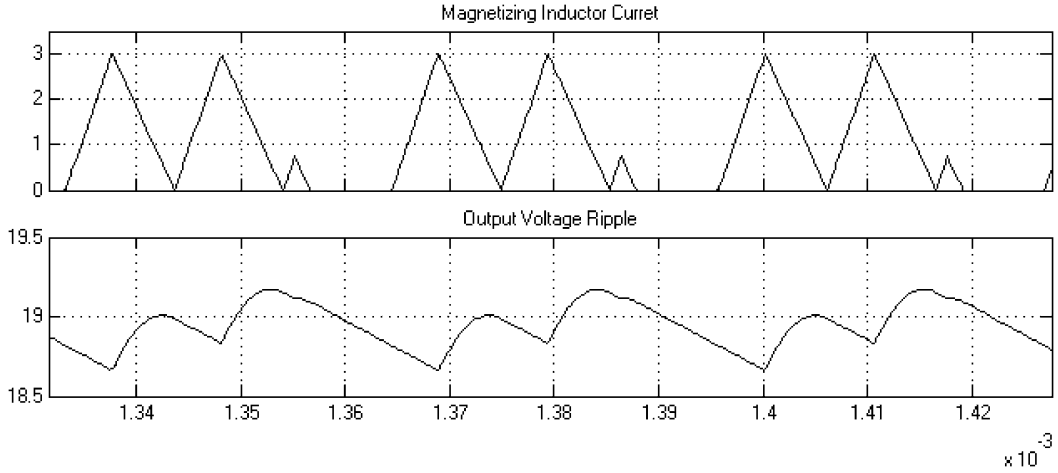

Fig. 3. Simulation results of the pulse train control of a typical flyback converter; (top) magnetizing inductor current (A) and (bottom) output voltage ripple (V) versus time (sec).

TABLE I
DEFINITION OF VARIABLES

Variable	Definition	Value
I_{max}	Peak current of the magnetizing inductance	3 A
L_m	Magnetizing inductance	225 µH
C	Output filter Capacitance	100 µF
R	Load resistance	-
V_{in}	Input voltage	150 V
V_{ref}	Output voltage reference	19 V
t_{on}	on time of the switch in a power pulse	-
t_{off}	off time of the switch in a power pulse	-
T	Switching period	-
k	ratio of the on time of the switch in a power pulse to the on time of the switch in a sense pulse	4
n	transformer turns ratio	6

where k is already defined in Table I. Therefore, in the closed loop control, the controller makes the decision of generating a power or a sense pulse, such that

$$\begin{aligned} V_{out} < V_{\rm ref} &\Rightarrow \Delta E_{\rm in} \\ &= 0.5 L_{\rm m} I_{\rm max}^2 \quad \text{Power Pulse} \\ V_{out} > V_{\rm ref} &\Rightarrow \Delta E_{\rm in} \\ &= 0.5 L_{\rm m} I_{\rm max}^2 k^2 \quad \text{Sense Pulse.} \end{aligned} \tag{11}$$

An example of the time-evolution of the sequence of power and sense pulses, in a closed loop system, based on (6) is depicted in Fig. 6.

In this figure, the energy level corresponding to $V_{\rm ref}$ is depicted as E_C^* and is equal to:

$$E_C^* = 0.5 C V_{\rm ref}^2. \tag{12}$$

As can be seen in Fig. 6, the closed loop system has two equilibrium points and the operation is oscillating between the two points. Both of the equilibrium points are stable. However, the operation between these two equilibrium points is oscillatory and yet stable. Because of this behavior, there are offsets from the reference signals. The output voltage ripple is a function of the circuit parameters.

IV. OUTPUT VOLTAGE RIPPLE

Stability analysis does not determine the output voltage ripple. Hence, the circuit differential equations need to be solved to predict the output voltage ripple. Considering the Flyback converter, in a power cycle, during the on time interval of the switch, the changes of the output voltage can be written as

$$\Delta v_{C(on)} \cong -\frac{V_{\rm ref}}{RC} t_{\rm on} = -\frac{V_{\rm ref}}{V_{\rm in}} \frac{L_{\rm m}}{RC} I_{\rm max}. \tag{13}$$

In the same cycle, assuming that the magnetizing current decreases linearly and the output voltage variation is small, the changes of the output voltage during the off time of the switch can be written as

$$\Delta v_{C(off)} \cong A(e^{-(t_{\rm off}/RC)} - 1) - \frac{R}{L_{\rm m}} V_{\rm ref} t_{\rm off} \tag{14}$$

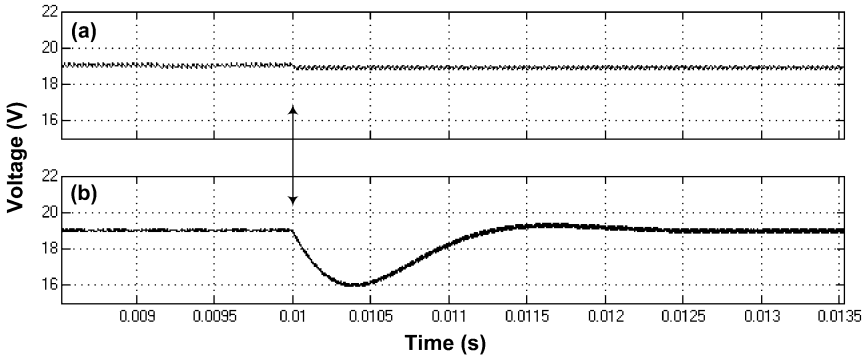

Fig. 4. Simulation results of the output voltage variation after a step load change of 30% to 65% of full-load: (a) pulse train and (b) PWM.

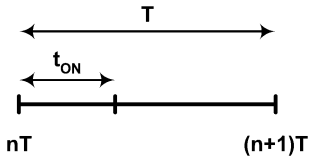

Fig. 5. General switching period.

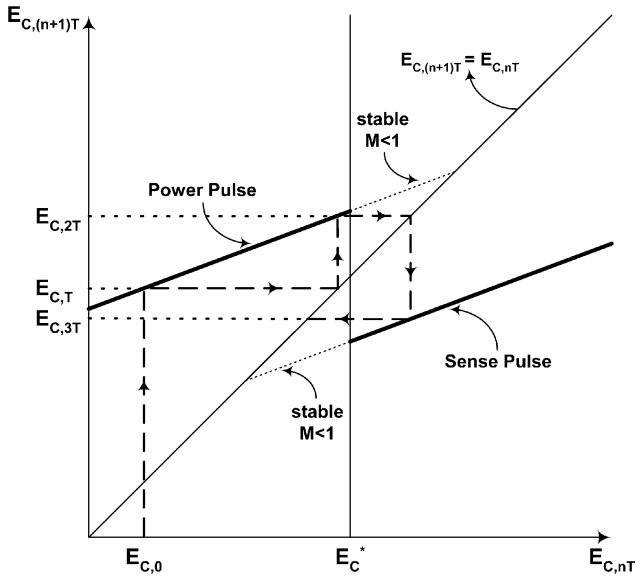

Fig. 6. Sequential evolution of power and sense pulses.

where $A = V_{\rm ref} - nRI_{\rm max} - (n^2R^2C/L_{\rm m})V_{\rm ref}$ and $t_{\rm off} = (L_{\rm m}I_{\rm max}/nV_{\rm ref})$.

The total changes of the output voltage after applying a power pulse is the summation of the above two extracted values and can be estimated as

$$\Delta v_{C,P} \cong \left(V_{\rm ref}\left(1-\frac{n^2R^2C}{L_{\rm m}}\right)-nRI_{\rm max}\right) \times \exp\left(-\frac{L_{\rm m}I_{\rm max}}{nRCV_{\rm ref}}\right) - V_{\rm ref}\left(1-\frac{n^2R^2C}{L_{\rm m}}+\frac{L_{\rm m}}{RC}\frac{I_{\rm max}}{V_{\rm in}}\right). \quad (15)$$

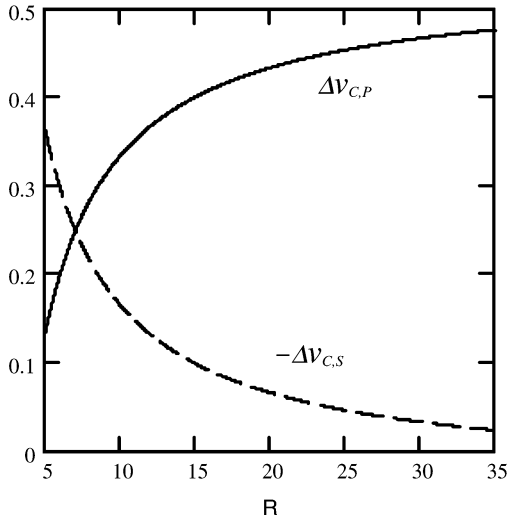

Fig. 7. $\Delta v_{C,P}$ (solid line) and $-\Delta v_{C,S}$ (dashed line) as functions of load resistance in flyback converter.

Continuing the same procedure for a sense cycle, we can easily get that the total changes of the output voltage after applying a sense pulse is equal to

$$\Delta v_{C,S} \cong \left(V_{\rm ref}\left(1-\frac{n^2R^2C}{L_{\rm m}}\right)-\frac{nRI_{\rm max}}{k}\right) \times \left(\exp\left(-\frac{L_{\rm m}I_{\rm max}}{nkRCV_{\rm ref}}\right)-1\right) - \frac{nRI_{\rm max}}{k} - \frac{L_{\rm m}I_{\rm max}}{RC}\left(\frac{V_{\rm ref}}{V_{\rm in}}+\frac{k-1}{nk}\right). \quad (16)$$

$\Delta v_{C,P}$ (solid line) and $-\Delta v_{C,S}$ (dashed line) as functions of the load resistance are sketched in Fig. 7. As we can observe, the control scheme tries to regulate the output voltage by generating the right number of sense and power pulses in each regulation cycle. As the output power increases, $\Delta v_{C,P}$ decreases; but, $-\Delta v_{C,S}$ increases. This fact implies that at a higher output power level, the control strategy prefers to have more power pulses rather than sense pulses in each regulation cycle and vice versa in light loads. The value of the output load resistance at which the two graphs cross each other is the value of load, which requires one power pulse associated with one sense pulse in each regulation cycle. The patterns of power and sense pulses in a regulation cycle for a specific value of the load resistance can be extracted using Fig. 7. Table II shows some examples of this case.

TABLE II
SENSE AND POWER PULSE PATTERN PREDICTION IN ONE REGULATION CYCLE

R	$\Delta v_{C,P}$	$-\Delta v_{C,S}$	Predicted Pattern
20	0.433	0.066	1*P - 7*S - 1*P - 6*S
15	0.400	0.099	1*P - 4*S
10	0.333	0.165	1*P - 2*S
7	0.249	0.249	1*P - 1*S
5	0.134	0.363	3*P - 1*S - 2*P - 1*S

According to Table II, for instance, when $R = 10$, we have $\Delta v_{C,P} \approx 2^* - \Delta v_{C,S}$ which predicts for this value of load, in each regulation cycle, the controller generates two sense pulses associated with each power pulse. Therefore, first we calculate $\Delta v_{C,P}$ and $-\Delta v_{C,S}$ ((15) and (16)) associated with each value of R, then we find two integers as this equation holds

$$\alpha * \Delta v_{C,P} = \beta * -\Delta v_{C,S} \tag{17}$$

where α and β represent the number of power and sense pulses in each regulation period. During the power cycle, we can express the average value of the diode current as

$$\overline{i_{D,P}} = \frac{nI_{\max}}{2}(1-d)T \tag{18}$$

where $d = (nV_O/V_{\text{in}} + nV_O)$ is the duty ratio. The on time of a sense pulse is $1/k$th of the on time of a power pulse and, hence, for a sense pulse, we can write

$$\overline{i_{D,S}} = \frac{\overline{i_{D,P}}}{k^2} = \frac{nI_{\max}}{2k^2}(1-d)T. \tag{19}$$

In the steady state operation, if there are α power pulses associated with β sense pulses in each regulation cycle, then the average value of the diode current is

$$\overline{i_D} = \frac{\alpha * \overline{i_{D,P}} + \beta * \overline{i_{D,S}}}{(\alpha+\beta)T}. \tag{20}$$

By noting that $\overline{i_D} = V_o/R$ and, by solving for the load resistance, one obtains

$$R = \frac{(\alpha+\beta)V_O}{\left(\alpha + \frac{\beta}{k^2}\right)\frac{I_{\max}}{2}\frac{nV_{\text{in}}}{V_{\text{in}}+nV_o}}. \tag{21}$$

Equation (21) shows how different parameters like input voltage, output voltage, output load resistance, $I_{\max}$, and k affect the pattern of power and sense pulses.

V. NEAR–ZERO–VOLTAGE SWITCHING

Sense pulses are being used to extract additional circuit information including transformer reset time and the instant at which the voltage across the switch is at its minimum level. This information is used to reduce the switch turn-on loss at the end of power pulses and, hence, improving the efficiency. Using an auxiliary winding, voltage across the isolating transformer is being monitored cycle by cycle. If required, the auxiliary winding can also provide power for the control circuitry.

Fig. 8 shows the voltage across the auxiliary winding in a sense pulse cycle. Pulse Train achieves low switch turn on loss

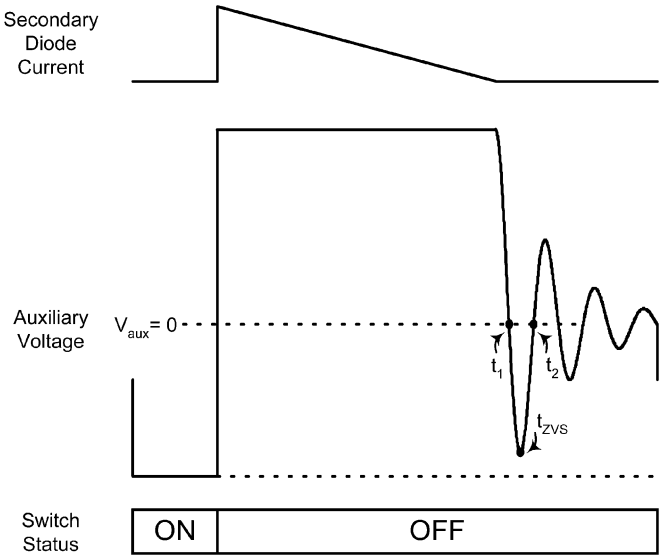

Fig. 8. Auxiliary voltage and zero voltage switching.

by using the resonance (ringing) that occurs after the current on the secondary side of the transformer reaches zero indicating the transition from power transfer to open-circuit conditions (Fig. 8). At the end of power pulses, the switch is turned on when the voltage across it is at its minimum level reducing turn-on losses. In addition, this switching point is always reached just after the transformer has reset allowing the circuit to operate very close to the critical conduction mode, where the switch is turned on immediately after reset optimizing circuit efficiency and reducing the size of the transformer.

As shown in Fig. 8, post-conduction resonance is a damped oscillation that falls very close to zero on its first cycle. Near-zero-voltage switching can simply be achieved by measuring the resonant period of the post conduction resonance on a sense cycle and turning the transistor on while its voltage is at the minimum level on the subsequent power cycles. On each power pulse, Pulse Train waits for the auxiliary voltage to drop below zero. This indicates that the converter is in the post-conduction resonance. After this event, the controller waits an additional ΔT that will take the voltage across the switch to its minimum level, then turns on the switch for the next cycle. In a sense pulse, the time between the zero-crossing on the auxiliary winding and the minimum primary voltage is estimated as being one-half the time between the negative-going zero crossing and the positive-going zero crossing, as shown in Fig. 8, $\Delta T = (t_2 - t_1)/2$. Given the geometry of the resonant signal, this estimate has high accuracy because this information is already measured during the last sense pulse.

By achieving near-zero-voltage switching, we also achieve critical conduction mode because we have turned the transistor back on immediately after the transformer's magnetic field has reset. This eliminates dead time between cycles and fully utilizes the output transformer. As a result, the transformer operates at lower flux levels than conventional converters resulting in lower core losses and, thus, higher efficiency.

Because the waveform is being monitored cycle-by-cycle, critical conduction mode is maintained across all variations in line and load conditions. In addition, this method of extracting

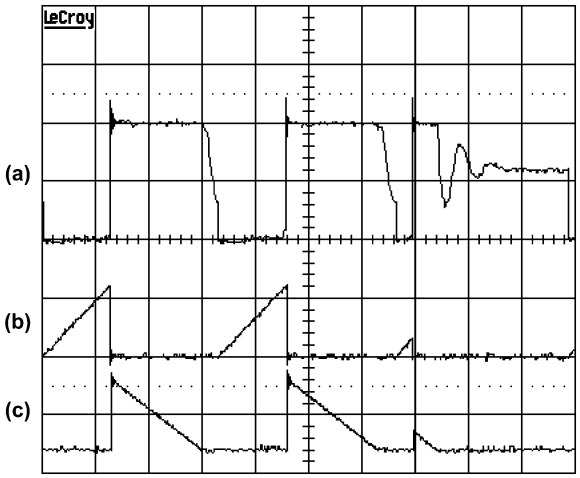

Fig. 9. Experimental results of (a) switch voltage (130 V/div), (b) primary current of transformer (2.5 A/div), and (c) secondary current of transformer (15 A/div).

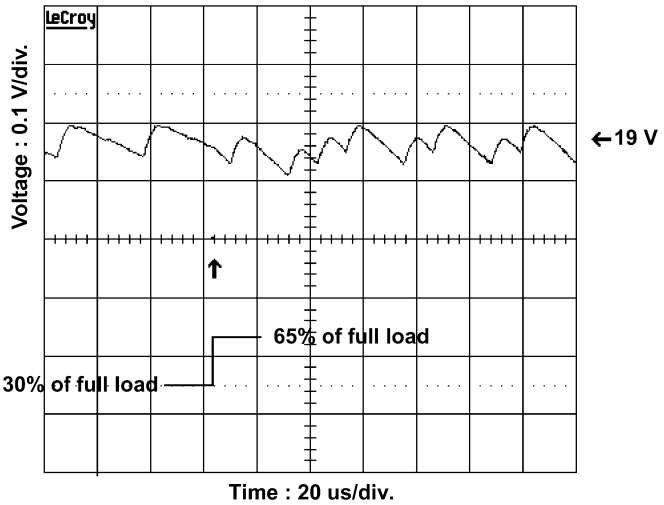

Fig. 10. Output voltage ripple for a step load change of 30% to 65% of full load.

maximum performance from the inductor is insensitive to component variations since the circuit behavior is measured, not assumed.

VI. Experimental Results

A 90-W prototype dc–dc Flyback power supply with $V_{\rm in} = 150$ V and $V_o = 19$ V was built and experimented using the developed IC (iW2201), which is a Pulse Train controller. The off time voltage across the switch in Flyback converter is equal to: $V_{\rm ds} = V_{\rm in} + n^*V_o$. Given the input and output voltages and choosing a 400 V switch to reduce the cost, n (transformer turns ratio) was chosen to be 6. This number will also make the current of magnetizing inductance $L_{\rm m}$ be nearly symmetric, hence, causing less current stress for the circuit components. The minimum value of the load resistance at full load is equal to $R_{\rm min} = V_o^2/P_{o,\rm max} = 4\Omega$ using (21) for $\beta = 0$ (full load condition) $I_{\rm max}$ can be calculated as $I_{\rm max} = 2.78$ A. $I_{\rm max} = 3$ A was chosen; this value also meets the switch current ratings. For $\alpha = 1$ and $\beta = 1$, the output power will approximately reduce to 50% of full load (compared to power pulses, sense pulses do not transfer that much power to the load). Solution of (21) for k, using this condition, suggests a ratio of 4 for this parameter. Magnetizing inductance $L_{\rm m}$ was chosen to be 245 μH to make the switching frequency equal to 90 kHz. Fig. 9 depicts the experimental results of the voltage across the switch and primary and secondary current of the transformer. In this figure, two power pulses followed by a sense pulse are shown. As can be observed in this figure, by choosing the right instant of turning on the switch, the voltage across the switch is reduced by 70%.

Fig. 10 depicts the experimental results of the output voltage ripple for a 30% to 65% step load change. The horizontal arrow shows the output voltage dc level, which is 19 V, whereas the vertical arrow specifies the instant at which the step change is applied.

VII. Smart-Skip Mode

As we already mentioned, the peak inductor current in a power pulse is k times the peak inductor current in a sense pulse; therefore, a sense pulse delivers $1/k^2$ as much power as a power pulse. A continuous stream of sense pulses thus delivers $100/k^2\%$ of the full load. If the load is lighter than this

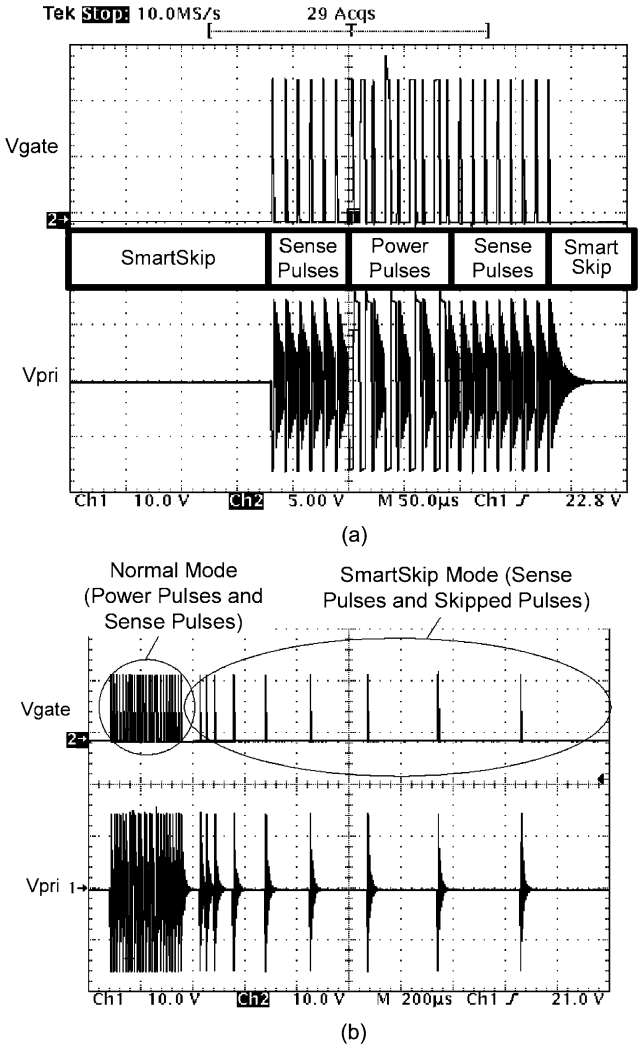

Fig. 11. (a) Experimental results of smart-skip and (b) the depth of smart-skip mode increasing with light load.

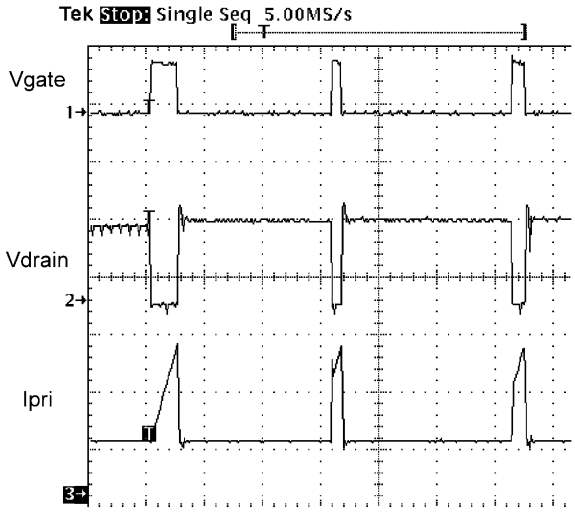

Fig. 12. Current limiting during start-up.

level, the controller enters *Smart-Skip Mode*, when the circuit alternates between the sense pulses and no pulses at all. This mode is similar to pulse skipping techniques.

The controller decides to enter the smart-skip mode when the sense pulses reveal that the output voltage is remaining above the desired level, though no power pulses have been sent recently [Fig. 11(a)]. The depth of the smart-skip mode (the ratio of skipped cycles to sense pulses) is increased or decreased according to the measured voltage and current in the skip-mode. The depth of the smart-skip mode needs to be reduced as the load resistance decreases [Fig. 11(b)].

VIII. Soft Start

Fig. 12 depicts the experimental signal waveforms at start-up. The first power pulse shows a clean current ramp; but, the drain voltage reflects the fact that the transformer does not reset by the time the second pulse arrives and, thus, operating in continuous conduction mode. This is also shown in the current on the second pulse, which starts at a nonzero value. However, the controller's peak current limiting causes the second power pulse to be much shorter than the first one. By the third cycle, the initial current has already fallen significantly due to the second cycle's shorter on time of the switch. This trend will continue until, in a few cycles, the initial current is zero and the converter is operating in discontinuous conduction mode.

IX. Conclusion

Flyback power converter has found its way into many applications. To address the challenge of designing a simple controller for this type of converters, this paper introduces the new Pulse Train control technique. This control method has several advantages over conventional techniques, such as simplicity, accuracy, and fast transient response. Simulation as well as experimental results completely match with the theoretical concept.

References

[1] R. E. Locher, "Introduction to power supplies," in *Proc. National Semiconductor Application Note 556*, Nov. 1988.

[2] P. Lidak, "Critical conduction mode flyback switching power supply using the MC33364," in *Proc. Motorola Semiconductor Application Note AN 1594*, 2003.

[3] G. Spiazzi, D. Tagliavia, and S. Spampinato, "dc–dc flyback converters in the critical conduction mode: A re-examination," in *Proc. IEEE Industry Applications Society Annual Meeting*, vol. 4, Rome, Italy, Oct. 2000, pp. 2426–2432.

[4] Motorola, "Critical Conduction GreenLine SMPS Controller," Tech. Rep. MC33364/D, Motorola, Inc., 1998.

[5] P. Luo, L. Luo, Z. Li, J. Yang, and G. Chen, "Skip cycle modulation in switching dc–dc converter," in *Proc. IEEE International Conference on Communications, Circuits and Systems and West Sino Expositions*, vol. 2, 2002, pp. 1716–1719.

[6] M. Telefus, A. Collmeyer, D. Wong, D. Manner, and Assignee: iWatt Corporation, "Switching power converter with gated oscillator controller," U.S. Patent 6 275 018, 2003.

[7] M. Telefus, D. Wong, C. Geber, and Assignee: iWatt Corporation, "Operating a power converter at optimal efficiency," U.S. Patent 6 304 473, 2003.

Mark Telefus received the M.S.E.E. degree from Tomsk University, Tomsk, Russia.

He has 27 years of corporate experience, including employment with Cyclotron Corporation, Systron-Donner, ASTEC, and ACER. For the12 years prior to his joining iWatt in 2000, he was a Consultant for Tandem, Ericsson/Raynet, Premisys, NEC, Go Corporation, Moto Development, and Nippon. His first experience in the United States was with Cyclotron Corporation where he developed the power control system for the main magnetizing RF D-structure. He joined the company in 1979 as an Engineer Scientist and helped on the first 45-rev cyclotron for cancer treatment and diagnosis. In 1983, he joined ASTEC and became one of the leading engineering forces to develop a new line of switching power supplies for Apple Computer. At ASTEC, he implemented the company's first products with shared regulation feedback, allowing for highly responsive transient response characteristics. He also joined ACER as the company's Director of new technology. His power supply designs allowed ACER to become a captive supplier of all power conversion products, helping the company increase operating margins. At ACER, he received three U.S. power conversion patents. As a Consultant, he was involved in numerous product developments in both the personal computer and telecom industries. His two U.S. patents with Ericsson/Raynet were incorporated in the first optical network unit for NYNEX. His development work for Premisys once again allowed the company to become a captive supplier of custom power supplies, enabling greater operating margins and better system performance. His power supply designs were incorporated in the first integrated access device for AT&T, Lucent, and MCI.

Anatoly Shteynberg (M'85) received the M.S. degree from the University of Dnepropetrovsk, Ukraine, in 1962 and the Ph.D. degree from ENIN University, Moscow, Russia, in 1969.

He was a Senior Researcher of the Academy of Sciences, U.S.S.R., and served as Acting Scientific Secretary of the Academic Institute of Cybernetics, Kishinev, Moldova, from 1971 through 1980, where he was involved in creation of national Power Electronics Industry of the U.S.S.R. In 1976, he published a book on independent invertors which was recommended by the High Education Ministry of the U.S.S.R. for all national universities as a manual for power electronics faculties. Since immigrating to the U.S., he has been holding Senior Engineering Management positions with IBM, Siemens, Ericson, Sipex, and iWatt. He has published more than 100 technical papers and books and has over 40 patents. His research interests included simulation models of power electronics, dc/ac converters, electrical motor drives, and control circuits.

Dr. Shteynberg is a member of IEEE Power Electronics Society.

Mehdi Ferdowsi (S'03) was born in Tehran, Iran, in 1974. He received the B.S. degree in electronics from the University of Tehran, Iran, in 1996, the M.S. degree in electrical engineering from Sharif University of Technology, Iran, in 1999, and is currently pursuing the Ph.D. degree in electrical engineering at the Illinois Institute of Technology, Chicago.

His research interests include digital control of switch mode power converters, dc–dc power converters, power factor correction circuits, and integrated power converters.

Mr. Ferdowsi received the 2003 Joseph J. Suozzi INTELEC Fellowship from the IEEE Power Electronics Society.

Ali Emadi (S'98–M'00–SM'03) received the B.S. and M.S. degrees in electrical engineering (with highest distinction) from the Sharif University of Technology, Tehran, Iran and the Ph.D. degree in electrical engineering from Texas A&M University, College Station.

In 1997, he was a Lecturer at the Electrical Engineering Department, Sharif University of Technology. He joined the Electrical and Computer Engineering Department, Illinois Institute of Technology (IIT), Chicago, in August 2000. He is the Director of Grainger Power Electronics and Motor Drives Laboratories, IIT, where he has established research and teaching laboratories as well as courses in power electronics, motor drives, and vehicular power systems. He is also the co-Founder and co-Director of IIT Consortium on Advanced Automotive Systems (ICAAS). He is the author of over 90 journal and conference papers as well as *Vehicular Electric Power Systems: Land, Sea, Air, and Space Vehicles* (New York: Marcel Dekker, 2003) and *Energy Efficient Electric Motors: Selection and Applications* (New York: Marcel Dekker, 2004). He is the Editor of the *Handbook of Automotive Power Electronics and Motor Drives* (New York: Marcel Dekker, 2004). He is a Member of the Editorial Board of the *Journal of Electric Power Components and Systems*. His main research interests include modeling, analysis, design, and control of power electronic converters/systems and motor drives, integrated converters, vehicular power electronics, and electric and hybrid electric propulsion systems.

Dr. Emadi received the Electric Power and Power Electronics Institute Fellowship for his graduate studies, the Best Paper Presentation Award from the IEEE 27th Industrial Electronics Conference, the 2002 University Excellence in Teaching Award from IIT, and the Overall Excellence in Research Award from the Office of the President, IIT, for mentoring undergraduate students. He directed a team of students to design and build a novel low-cost brushless dc motor drive for residential applications, which won the First Place Overall Award of the 2003 IEEE/DOE/DOD International Future Energy Challenge for Motor Competition. He is an Associate Editor of the IEEE TRANSACTIONS ON POWER ELECTRONICS. He is a Member of SAE and is listed in the International *Who's Who of Professionals* and *Who's Who in Engineering Academia*.